

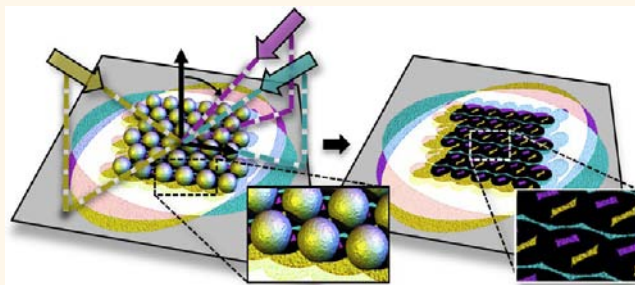
# Engineering Shadows to Fabricate Optical Metasurfaces

Alex Nemiroski,<sup>†</sup> Mathieu Gonidec,<sup>†</sup> Jerome M. Fox,<sup>†</sup> Philip Jean-Remy,<sup>†</sup> Evan Turnage,<sup>†</sup> and George M. Whitesides<sup>†,‡,§,\*</sup>

<sup>†</sup>Department of Chemistry & Chemical Biology, <sup>‡</sup>Wyss Institute for Biologically Inspired Engineering, and <sup>§</sup>The Kavli Institute for Bionano Science, Harvard University, Cambridge, Massachusetts 02138, United States

**ABSTRACT** Optical metasurfaces—patterned arrays of plasmonic nanoantennas that enable the precise manipulation of light–matter interactions—are emerging as critical components in many nanophotonic materials, including planar metamaterials, chemical and biological sensors, and photovoltaics. The development of these materials has been slowed by the difficulty of efficiently fabricating patterns with the required combinations of intricate nanoscale structure, high areal density, and/or heterogeneous composition.

One convenient strategy that enables parallel fabrication of periodic nanopatterns uses self-assembled colloidal monolayers as shadow masks; this method has, however, not been extended beyond a small set of simple patterns and, thus, has remained incompatible with the broad design requirements of metasurfaces. This paper demonstrates a technique—shadow-sphere lithography (SSL)—that uses sequential deposition from multiple angles through plasma-etched microspheres to expand the variety and complexity of structures accessible by colloidal masks. SSL harnesses the entire, relatively unexplored, space of shadow-derived shapes and—with custom software to guide multiangled deposition—contains sufficient degrees of freedom to (i) design and fabricate a wide variety of metasurfaces that incorporate complex structures with small feature sizes and multiple materials and (ii) generate, in parallel, thousands of variations of structures for high-throughput screening of new patterns that may yield unexpected optical spectra. This generalized approach to engineering shadows of spheres provides a new strategy for efficient prototyping and discovery of periodic metasurfaces.



**KEYWORDS:** nanophotonics · metasurfaces · nanoantennas · plasmonics · nanofabrication · nanosphere lithography · colloidal lithography · shadow-sphere lithography

This paper describes an efficient and versatile strategy for prototyping and discovery of periodic, optical metasurfaces—optically thin, nanostructured composites that enable the manipulation of light in ways not possible with naturally occurring materials.<sup>1</sup> Our approach, which we term shadow-sphere lithography (SSL), uses (i) sequential deposition from multiple angles through a self-assembled monolayer colloidal crystal (MCC) combined with (ii) a generalized, software-based approach to engineer plasmonic arrays formed by overlapping shadows of spheres. SSL enables a significant expansion in the range of patterns previously accessible by colloidal masks and yields myriad complex designs with feature-sizes, shapes, and compositions that are particularly advantageous for the development of nanophotonic materials.

Plasmonic metasurfaces, in particular, have the potential to revolutionize photonics by yielding on-chip, planar optical components, including frequency-selective surfaces,<sup>2,3</sup> linear and circular polarizers,<sup>4–7</sup> optical couplers,<sup>8</sup> beam steerers,<sup>9</sup> and planar lenses.<sup>3,10–12</sup> These materials have wide-reaching applications to tunable and nonlinear optics;<sup>13</sup> superresolution imaging;<sup>14</sup> light concentration for efficient solar harvesting and photodetection;<sup>15–18</sup> label-free, infrared, and single-molecule biological and chemical sensing and spectroscopy;<sup>19–23</sup> holography;<sup>24</sup> optical trapping;<sup>25–27</sup> and analog optical computation.<sup>28</sup> The exploration of these devices and the integration of theory and experiment to predict their performance in efficient, functional devices have been slowed by the difficulty of fabricating the intricate, finely featured arrays of plasmonic antennas that they require,

\* Address correspondence to gwhitesides@gmwhgroup.harvard.edu.

Received for review July 30, 2014 and accepted September 2, 2014.

Published online September 11, 2014  
10.1021/nn504214b

© 2014 American Chemical Society

both to collect empirical information and to test theory.

An optical metasurface comprises a two-dimensional (2D), patterned array of nanoantennas<sup>29</sup> that are composed of metals, semiconductors, and/or dielectrics and that couple to incident electromagnetic radiation (and often to one another) *via* surface plasmon resonances.<sup>30</sup> Theory predicts that this frequency-dependent response can be engineered—by controlling the size, shape, and composition of the antennas and arrangements of the unit cells in arrays—to manipulate the properties (such as amplitude, phase, and polarization) of scattered or localized light in an almost arbitrary way.<sup>1,6</sup> For periodic metasurfaces<sup>1</sup> (the subject of this work) the response is spatially uniform within the plane of the surface; for gradient metasurfaces<sup>31,32</sup> (which we do not consider here), such as those required to generate a flat lens, the unit cells, and therefore the frequency or phase responses, have a spatial dependence.

The only fabrication strategies that permit broad control over appropriate arrays (and then only incompletely) use conventional photo-, electron-beam, and or ion-beam lithography. These processes, however, are too expensive, too slow in moving from one pattern to another, and too limited in their ability to handle multiple materials to be useful for efficient exploration of this field. They are also entirely incompatible with the formation of large numbers of structures semirandomly. The ability to generate and explore the parameter space of patterns conveniently, empirically, and combinatorially would significantly increase the probability of discovering new optical phenomena.

One convenient alternative to conventional techniques for creating periodic patterns uses MCCs as stencils to produce fine (>20 nm), closely packed features, over relatively large areas (cm<sup>2</sup>). This method, which is commonly referred to as nanosphere lithography (NSL) or colloidal lithography,<sup>33</sup> was originally popularized by Van Duyne<sup>34</sup> to fabricate arrays of nanoparticles and later expanded by use of plasma etching to reduce the diameters of the spheres and by limited attempts at angled deposition and/or etching to yield simple variations.<sup>35–38</sup> The convenience of this method, however, has thus far been limited by the very narrow range of patterns it can produce and the lack of a capability to design new, complex structures; as a result, NSL has been incompatible with the broad design requirements of metasurfaces.

Here, we show that rationalizing the vast and almost entirely unexplored parameter space of shadow-derived shapes enables a substantial expansion of the spectrum of structures that can be generated by projection through MCCs. Our approach uses custom-designed software to engineer compositions of shadows that guide multiangled deposition of one

or multiple materials through a plasma-etched MCC. This simple, yet versatile strategy transforms an MCC into a nearly universal stencil that can produce an extensive variety of complex patterns that have not previously been realized physically or considered theoretically. To emphasize the central role that shadows of spheres (of any size) play in this approach to lithography, we adopt the name shadow-sphere lithography, which we believe appropriately describes this generalized technique.

We first demonstrate SSL as a method for rapidly prototyping periodic, optical metasurfaces with a wide range of constituent structures and material compositions that would be difficult to produce in any other way. We next explore SSL as a tool for empirical discovery of structures and optical phenomena by investigating a subset of patterns offered by a polycrystalline MCC with thousands of differently oriented domains per cm<sup>2</sup>. We finally assess the optical performance of SSL-produced structures by comparing the infrared transmission spectra of a subset of these metasurfaces with the spectra predicted by theory. The close agreement indicates that the spectral responses of these materials are relatively insensitive to the kinds of defects inherent to self-assembly. This work demonstrates SSL to be an operationally simple, generalizable method for efficient prototyping and discovery of new periodic metasurfaces active at near- to mid-infrared wavelengths.

## DESIGN OF METASURFACES WITH SSL

SSL enables the fabrication of these types of intricate patterns by overlapping the shadows cast in a beam of atoms or ions at multiple angles to an MCC. To help visualize these shadows, we first approximated the incident atomic flux by parallel, non-diffraction-limited rays and modeled the system (spheres, substrate, and sources of projection) in software used for ray tracing (MegaPOV).<sup>39</sup> Here, we use the term “projection” to describe collectively physical vapor deposition (PVD), directional etching (such as reactive ion etching, or RIE), or optical ray tracing (in the case of 3D computer rendering). The basic building block of a pattern designed by SSL is formed by a single angle of projection. For example, Figure 1a shows how the shadows of four, hexagonally non-close-packed (HNCP) spheres can overlap to form an isolated rectangular strip (“bar”) and how an array of HNCP spheres can generate an array of bars. These bars can take on many shapes and positions, which in turn depend on the four free parameters of the system (defined in Figure 1b): (i) the lattice constant or “pitch”, (ii) the width of the “gap” between the spheres, (iii) the polar (inclination) angle  $\theta$  of the source relative to the MCC, and (iv) the azimuthal (rotation) angle  $\phi$  of source relative to the MCC.

For a fixed gap and pitch and a single source of projection, the morphology of shapes can be tuned by

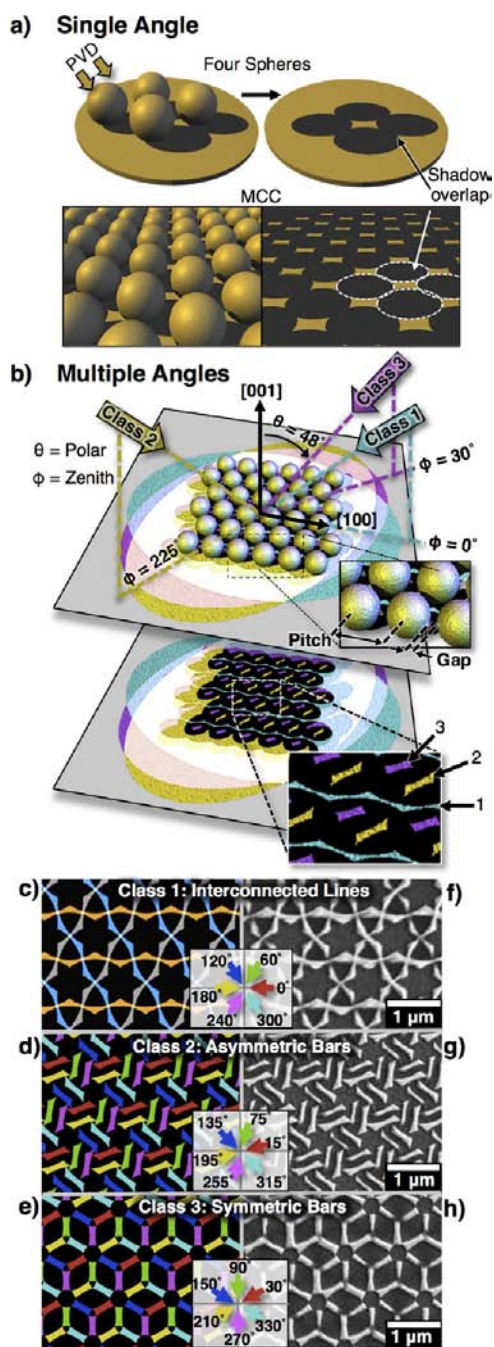


**Figure 1.** Schematic for single- and multiangled deposition. (a) Generation of a single bar or an array of bars by a single angle of deposition. (b) Definition of free parameters relative to the crystal axis. Here we show an example composed of three different types of features: (1) an interconnected line, (2) an asymmetric bar, and (3) a symmetric bar. (c–e) Composition of six angles of projection demonstrating the duplication of feature types 1–3 at intervals of  $\phi = 60^\circ$  due to the  $C_6$  symmetry of the lattice. (f–h) Images collected with a scanning electron microscope (SEM) of the fabricated versions of these patterns (20 nm of Ag on Si). Inset: The six angles by which the features are reproduced.

varying  $\theta$  and  $\phi$ . Through a comprehensive exploration of the space of available shadow-derived shapes, we have found that the patterns that result from different combinations of  $\theta$  and  $\phi$  generally belong to a set of

five classes: (1) interconnected lines, (2) asymmetric bars, (3) symmetric bars, (4) triangular islands, or (5) an interconnected, honeycomb-like lattice (Figures S1 and S2). Each feature can be duplicated at  $\phi = 60^\circ$  intervals due to the 6-fold ( $C_6$ ) rotation symmetry of the hexagonal lattice (Figure 1c–h). Varying the azimuthal angle  $\phi$  produces continuous transitions between the different classes of shadows and offers many intermediate positions and shapes; varying the polar angle  $\theta$  or the gap between the spheres controls position, length, and width of each of these features. We discuss this parameter space in greater detail in the Supporting Information (SI). Each theoretical parameter has an experimental analog: the pitch corresponds to the initial size of the spheres, the gap is tuned by reducing the diameters of spheres with oxygen plasma etching, and the angles of deposition are controlled with a rotation stage.

Although ray tracing is a useful tool for modeling shadows, the computation required is too slow to be used for rapid design. To accelerate this process, we modeled the shadow of each sphere as an ellipse projected onto the substrate. The positions, orientations, and aspect ratios of these elliptical shadows depend on the free parameters of the system (pitch, gap, and angles of projection) through simple mathematical relations (shown in the SI); multiple angles of projection can be easily and quickly modeled by overlapping the patterns produced by each individual angle.

We developed a Mathematica-based program, SSL Artist, that composes shadows produced from an arbitrary number of independent angles of projection (Figure S3). We have made a Web-based version of SSL Artist available online at [http://gmgwgroup.harvard.edu/science/SSL\\_artist/](http://gmgwgroup.harvard.edu/science/SSL_artist/). This design environment eliminates the need to consider the abstractions of multi-angled shadows and makes SSL broadly accessible by allowing users to design structures by “painting” a unit cell. Furthermore, we have enabled this software to guide designs that are specified by symmetry only. A user may specify the desired 2D point group (such as  $C_2$ ,  $C_6$ ,  $D_3$ , etc.) for a unit cell, and the software suggests patterns with the required symmetries for consideration, further editing, and fabrication (Figure S4). After finalizing a particular design, SSL Artist outputs the experimental parameters required for fabrication: the colloidal diameter, the etch recipe, and all angles of projection.

## DESIGN AND FABRICATION OF METASURFACES

The composition and structure of a unit cell can be designed by overlapping shapes produced from multiple angles of deposition. The various attributes (length, width, position, orientation, and interconnectedness) of each individual feature necessary to control the optical response of the array can be easily tuned

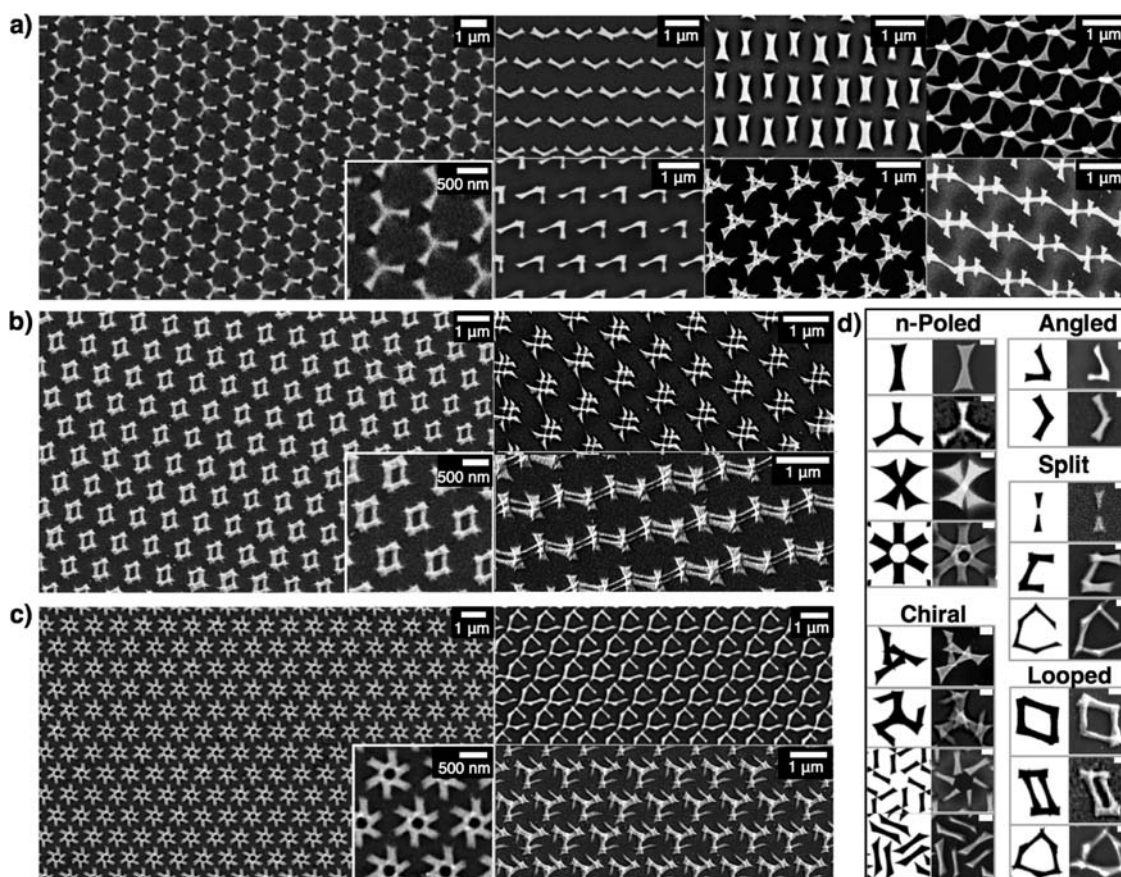


Figure 2. Nanoantennas designed and fabricated by SSL and imaged by a scanning electron microscope (SEM). (a–c) Patterns composed of two to three (a), four (b), and five to six (c) different angles of deposition. (d) Subset of possible unit cells categorized according to optical function as designed (left) and fabricated (right).

by varying the angles of deposition of each feature. Figures 2 and 3 show examples of nanoantennas and other nanopatterns composed of two to six different angles of deposition. Using SSL, we produced many of the most common morphologies of nanoantennas (such as connected n-poles, angled resonators, chiral resonators, split dipoles, split-ring resonators, and loop antennas). Figure 2d shows a subset of these nanoantennas categorized by optical function.

One of the major strengths of SSL is the simplicity with which multiple materials can be incorporated into the metasurface without removing the sample from the PVD chamber. This characteristic contrasts with the time-consuming and expensive steps (such as registration and additional lithography steps) that would be required to produce such materials with conventional methods. Any material that can be deposited by PVD can be used in SSL; each bar or interconnected line can correspond to a different material (or thickness of material). Figure 4 demonstrates this capability with patterns composed of two to six different materials that are commonly used for their plasmonic (Au, Ag, Cu), ferromagnetic (Ni, Co), antiferromagnetic (Cr), semiconducting (Ge), catalyzing (Pt, Co), or biomolecule immobilizing (Au) properties. We also include

more examples of other fabricated patterns that include multiple materials in Figure S6.

### CHARACTERIZATION OF POLYCRYSTALLINE METASURFACES

The method of crystallization that we used in this study formed MCCs that contained a large number ( $\sim 1500/\text{cm}^2$ ) of single-crystal domains with random orientations and areas that ranged from 0 to  $25 \text{ nm}^2$ . The availability of many large domains ( $\sim 500$  domains/ $\text{cm}^2$  with area  $> 100 \times 100 \text{ nm}^2$ ; Figure S7) yields many different patterns that can each be optically characterized. This polycrystalline distribution of domain orientations in a self-assembled MCC simplifies the SSL procedure by eliminating the need to orient samples carefully relative to the initial angle of deposition because the MCC naturally provides many correctly oriented domains. It also enables empirical fabrication of new patterns with unexpected structures by providing numerous orientations of domains that differ from those required for the target design. These misoriented domains usually form radically different patterns, each with a unique optical spectrum.

The shapes produced within different domains provide an important opportunity for the discovery of new

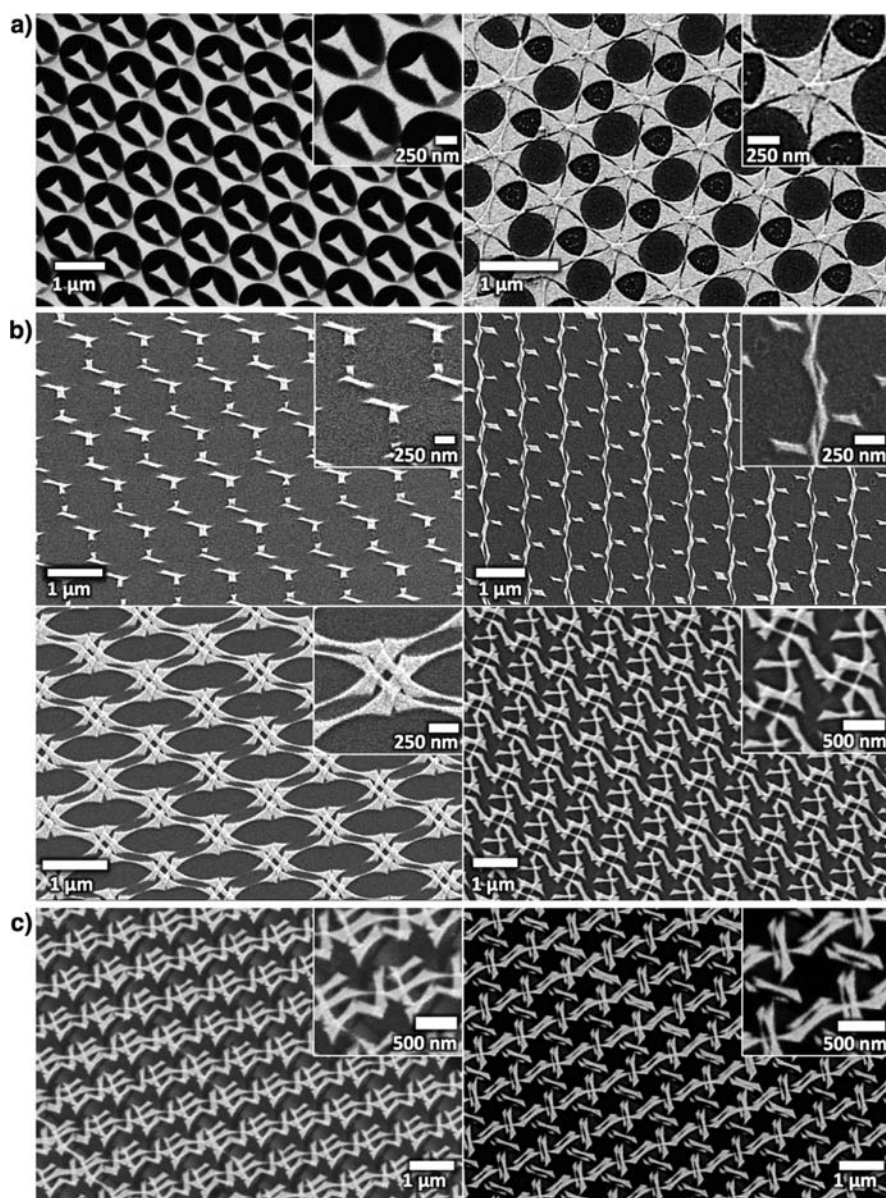
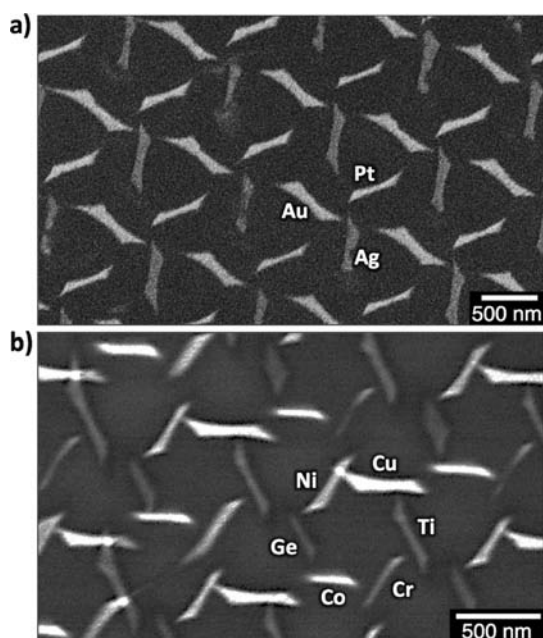


Figure 3. Examples of complex nanopatterns accessible with SSL using two to three (a), four to five (b), and six (c) different angles of deposition. Images were acquired by SEM.

nano-optical patterns, and they can be easily predicted predeposition and/or rationalized postdiscovery. For example, for a target design that consists of a set of angles of deposition  $\{\theta_i, \phi_i\}$  relative to the [100] axis of a chosen domain, the shadows produced within any misoriented domains can be modeled by subtracting a misorientation angle  $\phi_0$  from the original azimuthal angles (that is,  $\{\theta_i, \phi_i\} \rightarrow \{\theta_i, \phi_i - \phi_0\}$ ). This extra free parameter enables the prediction of all possible structures formed within a polycrystalline sample; alternatively, once an interesting pattern is observed, a quick search of the parameter space yields the angular offsets associated with that pattern.

To demonstrate the opportunity for discovery presented by polycrystalline MCCs, we designed an array of four-sided, “looped” nanoantennas (Figure 5a) in

SSL Artist. We then fabricated these patterns by depositing metal (2 nm Ti/20 nm Au) sequentially, at the four angles specified by our design, through an MCC of polystyrene microspheres (1  $\mu\text{m}$  pitch, 122 nm gap) on a borosilicate substrate. We chose to characterize three representative domains (Figure 5b): one that matched the orientation specified by our design ( $\phi_0 = 0$ ) and two others that corresponded to  $\phi_0 = 20^\circ$  and  $\phi_0 = 33^\circ$ . We used SEM to identify these domains and Fourier transform infrared spectroscopy (FTIR) to measure their transmission spectra. The shapes produced by these domains could be easily predicted by the SSL software (Figure 5c–h), and their transmission spectra agreed well with simulations performed by finite integration technique (Figure 5i–n). Although there are thousands of variations of these patterns



**Figure 4.** Multimaterial structures. (a) SEM images of an array of chiral, tripolar structures (formed by three asymmetric bars) fabricated with each bar composed of 20 nm of Au, Ag, or Pt. (b) Array of chiral, hexagonal structures (formed by six asymmetric bars) fabricated with each bar composed of 10 nm of either Cu, Ti, Cr, Co, Ge, or Ni.

formed on the polycrystalline substrate, all structures belong to three qualitative families (e.g., Figures 1c–h) due to the  $C_6$  symmetry of the hexagonal lattice. We specifically chose these three examples because they are typical representatives of the three families of shapes; all other domains contained patterns that were intermediate between the ones shown.

## DISCUSSION

The range of designs accessible *via* an HNCP array of spheres suggests that it provides a nearly universal stencil for two reasons: (i) the small contact area of a sphere resting on a flat substrate obscures very little of the underlying substrate from the “line of sight” associated with some subset of angles, and, thus, most areas can be patterned, and (ii) the fill factor of an HNCP array of spheres offers a high areal density of narrow gaps for casting and overlaying many different shadows. These characteristics enable a sphere-based shadow mask to pattern nearly anywhere within the unit cell (although the gaps available to project patterns are restricted to the  $\rho 6m$  symmetry of the array). This colloidal mask requires a minimum of customization (only plasma etching), and the method as a whole requires a relatively uncomplicated modification to a common commercial system (the installation of a dual-axis rotation stage into an e-beam evaporator).

In this work, we have used microspheres to fabricate patterns that primarily resonate at near- to mid-infrared wavelengths because this spectral region has many important applications in telecommunications,

chemical sensing, solar energy harvesting, and thermal management. For other applications, it may be possible to access the visible spectrum by choosing steeper polar angles to produce smaller nanoantennas or by reducing the periodicity and size of the nanoantennas by using smaller colloidal spheres (e.g., 0.1–0.5  $\mu\text{m}$ ), which are commercially available and can be readily self-assembled into MCCs.

There are four aspects of shadow-based deposition through a self-assembled stencil that can cause fabricated metasurfaces to differ from the idealized geometry of a perfectly periodic array of identical nanoantennas with constant thickness: (i) material buildup on the spheres narrows the gaps and can distort features; (ii) overlap between different features produces a nonflat topography; (iii) imperfect packing and nonuniform sphere size introduce defects and random variations within each grain; and (iv) the diverging flux of the incident material from an uncollimated source imposes a gradient in the size of features across a sample. With a proper understanding of the system, however, each of these effects can be mitigated or at least predicted.

Material buildup on the spheres from the deposition of one feature may distort the shape of a subsequent feature projected through the same gap and may influence the plasmonic resonances of different features within the unit cell. This effect can be distributed more evenly to all features by depositing less material at a time and building up the thickness of each feature in succession. For example, for the parallelogram metasurface that we optically characterized, we first deposited 10 nm of material at each of the four angles specified to form the four sides of the parallelogram. We then repeated the same sequence a second time to reach the desired 20 nm thickness for each of the four features. This procedure did not reduce the material buildup overall, but distributed its effect more evenly across all features.

The narrowing of gaps between spheres produces a slight taper in the thickness of deposited features, and the overlap of adjacent features causes thickened topographies at the intersections between features. These effects combine to produce a 3D topography that departs from the idealized flat structures employed in our simulations; when, however, we corrected the simulations using an effective thickness (15 nm) of deposited material, the simulated spectra agreed well with measured spectra (as shown in Figure 5i–n). In general, we observed that these structural distortions and nonconstant thickness primarily shift the entire spectrum slightly ( $\sim 100$ – $200$  nm) to the red. This shift can be predicted and accommodated in the simulations *via* the alteration of a single parameter (the material thickness).

The crystallographic defects inherent to self-assembly (vacancies, dislocations, and grain boundaries) appear to

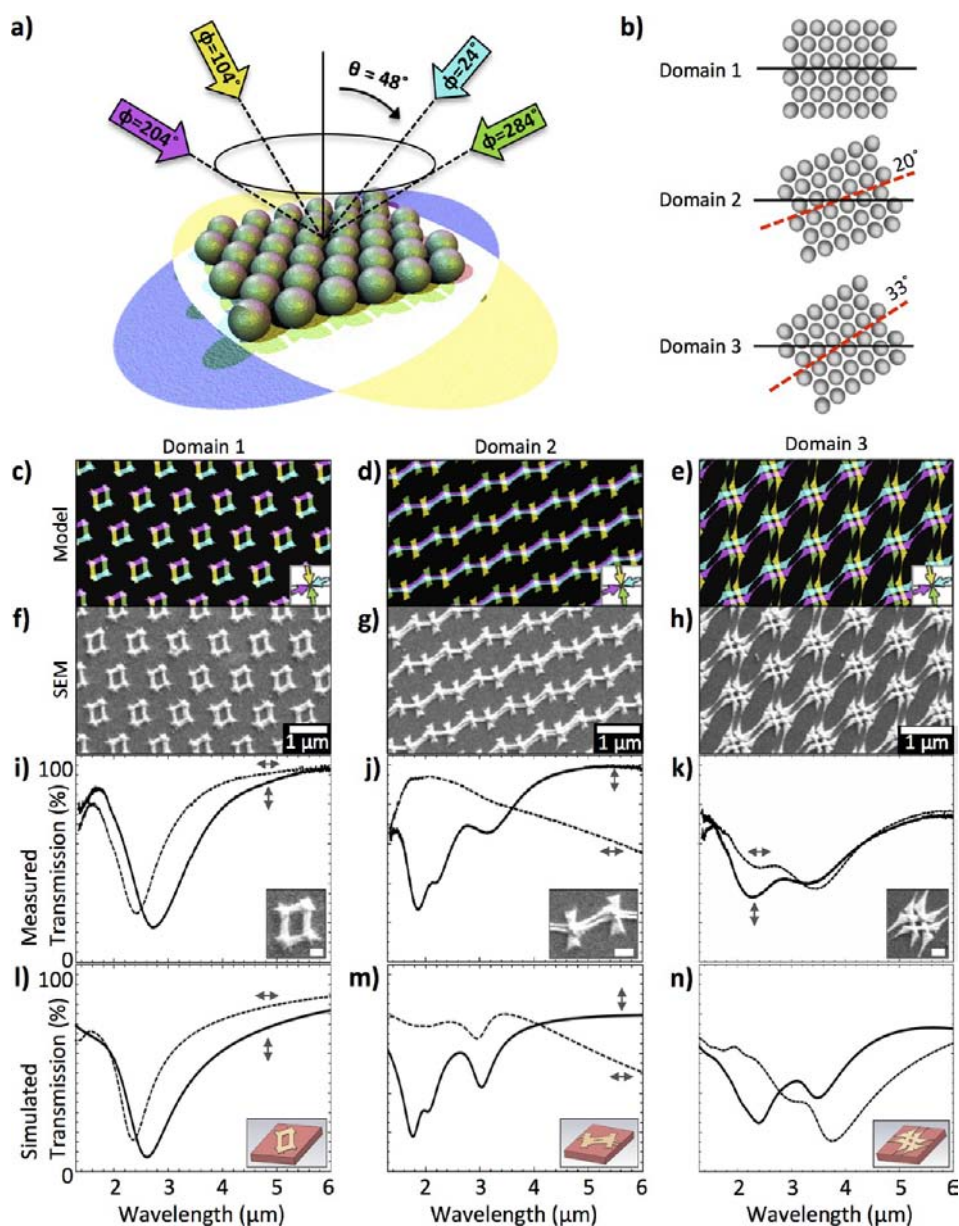


**Figure 5.** Morphology and transmission spectrum of different domains on the same polycrystalline MCC. (a) A 3D scheme for the four angles of deposition used to produce the array of a four-sided “looped” array of nanoantennas. (b) Orientation (relative to the initial design) of three domains on the same substrate that we chose to characterize. (c–e) Modeled domains. (f–h) SEM images of the fabricated domains. (i–k) FTIR transmission spectra of the fabricated domains. The incident polarizations (relative to the SEM images in f–h) are labeled near each spectrum. Scale bars on the inset figures represent 200 nm. (l–n) Simulated transmission spectra. Inset figures show the simulated unit cells.

have little effect on the optical spectra of single domains; they marginally reduce the overall intensity of the transmission spectrum, relative to a theoretically perfect array, and do not significantly alter the spectral shape.

Both nonuniform sizes of the microspheres and the use of an uncollimated source can cause variations in the size of shadow-derived features: nonuniform sphere sizes lead to random variations; the divergent flux of incident material, by contrast, leads to a smooth gradient across the sample. In our geometry, the distance between the source of deposition and the sample was 33 cm, which yielded a gradient in the

polar angle of  $\leq 0.2^\circ/\text{mm}$ ; across a typical grain of diameter of  $\sim 1$  mm, this variation distorted the length of features by  $\leq 0.5\%$  relative to the expected size. These random and gradual variations within each grain lead to inhomogeneous broadening of the experimental spectra as compared with the theoretical spectrum. If necessary, these effects can be reduced by filtering the spheres to attain greater uniformity, by moving the sample farther away from the source of deposition to narrow the solid angle of the incident flux, and/or by adding a collimating apparatus to reduce the angular divergence of the incident flux.

Despite the various nonidealities inherent to this technique, the close match between theory and experiment indicates that optical spectra of metasurfaces generated by SSL are either insensitive to or predictably sensitive to these effects. Although beyond the scope of the present work, future efforts could account for such nonidealities by employing algorithms that incorporate material buildup and other sources of variation into the modeling of shadows and simulations of optical spectra.

## CONCLUSIONS

SSL enables the efficient design and fabrication of two-dimensional arrays of complex, high-density, multimaterial structures by harnessing the parallelism of bottom-up self-assembly, the rationality of software-aided design, and the precision of top-down physical vapor deposition. This approach has several characteristics that make it advantageous for the development of metasurfaces. SSL makes it simple to design new, sophisticated patterns and to fabricate them rapidly (~hours). It provides an opportunity to design nanoantennas by topological symmetry only and to discover new metasurfaces by allowing nature to provide a continuum of unique variations on designed patterns, each resulting from a different domain orientation. SSL also opens new avenues in nano-optics by easily producing nanoantennas with important attributes that are necessary to engineer optically interesting behavior including (but not restricted to) (i) extremely sharp features (down to 10 nm radius of curvature) and small gaps (down to 20 nm) for strong localization of electric fields or “hot spots”; (ii) centrosymmetric shapes that could focus light with orbital angular momentum,<sup>40</sup> (iii) non-centrosymmetric shapes to couple to linearly polarized light; (iv) chiral shapes to couple to circularly polarized light; (v) looped shapes to couple to the magnetic modes; (vi) structures with

broken symmetries to generate Fano resonances,<sup>41</sup> (vii) interconnected patterns that can be used to address active devices; and (viii) meta-molecules with building units that can include spatial variation in material thickness and/or composition. Beyond metasurfaces, these characteristics are also attractive for the fabrication of other materials as well. For example, SSL can produce patterned arrays that could include phase-change materials for applications in data storage;<sup>42</sup> ferro- or anti-ferromagnetic constituents for spintronic or magnonic devices,<sup>43,44</sup> artificial spin ice,<sup>45</sup> topological insulators,<sup>46</sup> or magnetically directed colloidal assembly;<sup>47</sup> catalytic sites for chemical growth;<sup>48</sup> immobilization sites for biochemical sensing;<sup>20,22</sup> or ultranarrow gaps for studying quantum plasmon resonances.<sup>49</sup>

Shadow-based deposition through a self-assembled mask also presents several challenges that include (i) better management of the various sources of distortion, (ii) improving the quality of colloidal crystals, (iii) producing smaller nanoantennas with higher planar densities to access the visible spectrum, and (iv) expanding the accessible classes of shapes and array geometries. In the future, these challenges may be overcome by adjusting angular deposition dynamically (with a computer-controlled rotation stage), by incorporating nonspherical occluding objects (such as cubes, which would cast parallelogrammatic shadows), and/or by employing a template to direct self-assembly. These developments may yield new classes of shapes, high-quality wafer-scale domains, and gradients in material thickness and may also extend SSL beyond periodic metasurfaces toward more sophisticated patterns such as optical phase gradients to shape wavefronts.<sup>32</sup> By bridging the two iteratively linked halves of metasurface development—theory and experiment—SSL promises to accelerate the pace of design, fabrication, and discovery in fields including metamaterials, nano-optics, nanomagnetism, and biosensing.

## METHODS

We first designed all patterns with SSL Artist. We then fabricated MCCs composed of polystyrene spheres with 1  $\mu\text{m}$  diameter at an air/water interface, deposited them on bare silicon wafers, and performed an isotropic etch with oxygen plasma to reduce the diameter of the spheres,<sup>50</sup> thereby opening the gaps to our design specifications. Finally, we mounted each sample onto a custom-built, dual-axis rotation stage and adjusted the relative angle between the sample and source of deposition, for each angle of deposition, as specified by our designs. We include further details on the design of the software, rotation stage, and fabrication procedure in the SI.

*Conflict of Interest:* The authors declare no competing financial interest.

*Acknowledgment.* We thank N. Vogel, S. Kostinski, B. Chen, and K. Brown for useful discussions. This work was primarily supported by the Office of Naval Research under award no. N00014-10-1-0942 (A.N. and J.M.F.). Further support was provided by Marie Curie project SAM-TunEGaln:OF-2012-328412

(M.G.) and the National Science Foundation (NSF) under award nos. DMR-0820484 (E.T.) and DMR-1262895 (P.J.). This work was performed in part at the Center for Nanoscale Systems (CNS), a member of the National Nanotechnology Infrastructure Network (NNIN), which is supported by NSF award no. ECS-0335765. CNS is part of Harvard University.

*Supporting Information Available:* Extended background, theoretical discussion, description of SSL Artist software, materials and methods, results, and characterization. This material is available free of charge via the Internet at <http://pubs.acs.org>.

## REFERENCES AND NOTES

- Holloway, C. L.; Kuester, E. F.; Gordon, J. A.; O'Hara, J.; Booth, J.; Smith, D. R. An Overview of the Theory and Applications of Metasurfaces: The Two-Dimensional Equivalents of Metamaterials. *IEEE Ant. Prop. Mag.* **2012**, *54*, 10–35.
- Li, P.-C.; Zhao, Y.; Alù, A.; Yu, E. T. Experimental Realization and Modeling of a Subwavelength Frequency-Selective Plasmonic Metasurface. *Appl. Phys. Lett.* **2011**, *99*, 221106–221106–3.



3. Memarzadeh, B.; Mosallaei, H. Layered Plasmonic Tripods: an Infrared Frequency Selective Surface Nanofilter. *J. Opt. Soc. Am. B* **2012**, *29*, 2347–2351.
4. Ellenbogen, T.; Seo, K.; Crozier, K. B. Chromatic Plasmonic Polarizers for Active Visible Color Filtering and Polarimetry. *Nano Lett.* **2012**, *12*, 1026–1031.
5. Zhao, Y.; Alù, A. Manipulating Light Polarization with Ultrathin Plasmonic Metasurfaces. *Phys. Rev. B* **2011**, *84*, 205428.
6. Kats, M. A.; Genevet, P.; Aoust, G.; Yu, N.; Blanchard, R.; Aieta, F.; Gaburro, Z.; Capasso, F. Giant Birefringence in Optical Antenna Arrays with Widely Tailorable Optical Anisotropy. *Proc. Natl. Acad. Sci. U.S.A.* **2012**, *109*, 12364–12368.
7. Yu, N.; Aieta, F.; Genevet, P.; Kats, M. A.; Gaburro, Z.; Capasso, F. A Broadband, Background-Free Quarter-Wave Plate Based on Plasmonic Metasurfaces. *Nano Lett.* **2012**, *12*, 6328–6333.
8. Lin, J.; Mueller, J. B.; Wang, Q.; Yuan, G.; Antoniou, N.; Yuan, X.-C.; Capasso, F. Polarization-Controlled Tunable Directional Coupling of Surface Plasmon Polaritons. *Science* **2013**, *340*, 331–334.
9. Shegai, T.; Chen, S.; Miljković, V. D.; Zengin, G.; Johansson, P.; Käll, M. A Bimetallic Nanoantenna for Directional Colour Routing. *Nat. Commun.* **2011**, *2*, 481.
10. Verslegers, L.; Catrysse, P. B.; Yu, Z.; White, J. S.; Barnard, E. S.; Brongersma, M. L.; Fan, S. Planar Lenses Based on Nanoscale Slit Arrays in a Metallic Film. *Nano Lett.* **2008**, *9*, 235–238.
11. Aieta, F.; Genevet, P.; Kats, M. A.; Yu, N.; Blanchard, R.; Gaburro, Z.; Capasso, F. Aberration-Free Ultrathin Flat Lenses and Axicons at Telecom Wavelengths Based on Plasmonic Metasurfaces. *Nano Lett.* **2012**, *12*, 4932–4936.
12. Ni, X.; Ishii, S.; Kildishev, A. V.; Shalaev, V. M. Ultra-Thin, Planar, Babinet-Inverted Plasmonic Metalenses. *Light Sci. Appl.* **2013**, *2*, e72.
13. Zheludev, N. I.; Kivshar, Y. S. From Metamaterials to Metadevices. *Nat. Mater.* **2012**, *11*, 917–924.
14. Chen, P.-Y.; Alù, A. Subwavelength Imaging Using Phase-Conjugating Nonlinear Nanoantenna Arrays. *Nano Lett.* **2011**, *11*, 5514–5518.
15. Atwater, H. A.; Polman, A. Plasmonics for Improved Photovoltaic Devices. *Nat. Mater.* **2010**, *9*, 205–213.
16. Chalabi, H.; Schoen, D.; Brongersma, M. L. Hot-Electron Photodetection with a Plasmonic Nanostripe Antenna. *Nano Lett.* **2014**, *14*, 1374–1380.
17. Kim, S. J.; Thomann, I.; Park, J.; Kang, J. H.; Vasudev, A. P. Light Trapping for Solar Fuel Generation with Mie Resonances. *Nano Lett.* **2014**, *14*, 1446–1452.
18. Brongersma, M. L.; Cui, Y.; Fan, S. Light Management for Photovoltaics Using High-Index Nanostructures. *Nat. Mater.* **2014**, *13*, 451–460.
19. Yanik, A. A.; Cetin, A. E.; Huang, M.; Artar, A.; Mousavi, S. H.; Khanikaev, A.; Connor, J. H.; Shvets, G.; Altug, H. Seeing Protein Monolayers with Naked Eye Through Plasmonic Fano Resonances. *Proc. Natl. Acad. Sci. U.S.A.* **2011**, *108*, 11784–11789.
20. Liu, N.; Tang, M. L.; Hentschel, M.; Giessen, H.; Alivisatos, A. P. Nanoantenna-Enhanced Gas Sensing in a Single Tailored Nanofocus. *Nat. Mater.* **2011**, *10*, 631–636.
21. Xu, X.; Peng, B.; Li, D.; Zhang, J.; Wong, L. M.; Zhang, Q.; Wang, S.; Xiong, Q. Flexible Visible–Infrared Metamaterials and Their Applications in Highly Sensitive Chemical and Biological Sensing. *Nano Lett.* **2011**, *11*, 3232–3238.
22. Wu, C.; Khanikaev, A. B.; Adato, R.; Arju, N.; Yanik, A. A.; Altug, H.; Shvets, G. Fano-Resonant Asymmetric Metamaterials for Ultrasensitive Spectroscopy and Identification of Molecular Monolayers. *Nat. Mater.* **2012**, *11*, 69–75.
23. Kravets, V. G.; Schedin, F.; Jalil, R.; Britnell, L.; Gorbachev, R. V.; Ansell, D.; Thackray, B.; Novoselov, K. S.; Geim, A. K.; Kabashin, A. V. Singular Phase Nano-Optics in Plasmonic Metamaterials for Label-Free Single-Molecule Detection. *Nat. Mater.* **2013**, *12*, 304–309.
24. Ni, X.; Kildishev, A. V.; Shalaev, V. M. Metasurface Holograms for Visible Light. *Nat. Commun.* **2013**, *4*, 2807–2807.
25. Juan, M. L.; Righini, M.; Quidant, R. Plasmon Nano-Optical Tweezers. *Nat. Photonics* **2011**, *5*, 349–356.
26. Roxworthy, B. J.; Ko, K. D.; Kumar, A.; Fung, K. H.; Chow, E. K.; Liu, G. L.; Fang, N. X.; Toussaint, K. C., Jr. Application of Plasmonic Bowtie Nanoantenna Arrays for Optical Trapping, Stacking, and Sorting. *Nano Lett.* **2012**, *12*, 796–801.
27. Gullans, M.; Tiecke, T. G.; Chang, D. E.; Feist, J.; Thompson, J. D.; Cirac, J. I.; Zoller, P.; Lukin, M. D. Nanoplasmonic Lattices for Ultracold Atoms. *Phys. Rev. Lett.* **2012**, *109*, 235309.
28. Silva, A.; Monticone, F.; Castaldi, G.; Galdi, V.; Alù, A.; Engheta, N. Performing Mathematical Operations with Metamaterials. *Science* **2014**, *343*, 160–163.
29. Krasnok, A. E.; Maksymov, I. S.; Denisyuk, A. I.; Belov, P. A.; Miroshnichenko, A. E.; Simovski, C. R.; Kivshar, Y. S. Optical Nanoantennas. *Phys.-Usp.* **2013**, *56*, 539.
30. Giannini, V.; Fernandez-Dominguez, A. I.; Heck, S. C.; Maier, S. A. Plasmonic Nanoantennas: Fundamentals and Their Use in Controlling the Radiative Properties of Nanoemitters. *Chem. Rev.* **2011**, *111*, 3888–3912.
31. Kildishev, A. V.; Boltasseva, A.; Shalaev, V. M. Planar Photonics with Metasurfaces. *Science* **2013**, *339*, 1289–1289.
32. Yu, N.; Capasso, F. Flat Optics with Designer Metasurfaces. *Nat. Mater.* **2014**, *13*, 139–150.
33. Yu, Y.; Zhang, G. Colloidal Lithography. In *Updates in Advanced Lithography*; Hosaka, S., Ed.; InTech, 2013.
34. Hulteen, J. C.; Van Duyne, R. P. Nanosphere Lithography: a Materials General Fabrication Process for Periodic Particle Array Surfaces. *J. Vac. Sci. Technol. A* **1995**, *13*, 1553–1558.
35. Kosioerek, A.; Kandulski, W.; Chudzinski, P.; Kempa, K.; Giersig, M. Shadow Nanosphere Lithography: Simulation and Experiment. *Nano Lett.* **2004**, *4*, 1359–1363.
36. Choi, Y.; Hong, S.; Lee, L. P. Shadow Overlap Ion-Beam Lithography for Nanoarchitectures. *Nano Lett.* **2009**, *9*, 3726–3731.
37. Zhao, J.; Frank, B.; Burger, S.; Giessen, H. Large-Area High-Quality Plasmonic Oligomers Fabricated by Angle-Controlled Colloidal Nanolithography. *ACS Nano* **2011**, *5*, 9009–9016.
38. Vogel, N.; Fischer, J.; Mohammadi, R.; Retsch, M.; Butt, H.-J.; Landfester, K.; Weiss, C. K.; Kreiter, M. Plasmon Hybridization in Stacked Double Crescents Arrays Fabricated by Colloidal Lithography. *Nano Lett.* **2011**, *11*, 446–454.
39. MegaPOV Web site <http://megapov.inetart.net/> (accessed Feb 24, 2014).
40. Heeres, R. W.; Zwiller, V. Subwavelength Focusing of Light with Orbital Angular Momentum. *Nano Lett.* **2014**, *14*, 4598–4601.
41. Luk'yanchuk, B.; Zheludev, N. I.; Maier, S. A.; Halas, N. J.; Nordlander, P.; Giessen, H.; Chong, C. T. The Fano Resonance in Plasmonic Nanostructures and Metamaterials. *Nat. Mater.* **2010**, *9*, 707–715.
42. Wuttig, M.; Yamada, N. Phase-Change Materials for Rewriteable Data Storage. *Nat. Mater.* **2007**, *6*, 824–832.
43. Chappert, C.; Fert, A.; Van Dau, F. N. The Emergence of Spin Electronics in Data Storage. *Nat. Mater.* **2007**, *6*, 813–823.
44. Yu, H.; Duerr, G.; Huber, R.; Bahr, M.; Schwarze, T.; Brandl, F.; Grundler, D. Omnidirectional Spin-Wave Nanograting Coupler. *Nat. Commun.* **2013**, *4*, 2702–2702.
45. Zhang, S.; Gilbert, I.; Nisoli, C.; Chern, G.-W.; Erickson, M. J.; O'Brien, L.; Leighton, C.; Lammert, P. E.; Crespi, V. H.; Schiffer, P. Crystallites of Magnetic Charges in Artificial Spin Ice. *Nature* **2013**, *500*, 553–557.
46. Nagaosa, N.; Tokura, Y. Topological Properties and Dynamics of Magnetic Skyrmions. *Nat. Nanotechnol.* **2013**, *8*, 899–911.
47. Demirörs, A. F.; Pillai, P. P.; Kowalczyk, B.; Grzybowski, B. A. Colloidal Assembly Directed by Virtual Magnetic Moulds. *Nature* **2013**, *503*, 99–103.
48. Noorduyn, W. L.; Grinthal, A.; Mahadevan, L.; Aizenberg, J. Rationally Designed Complex, Hierarchical Microarchitectures. *Science* **2013**, *340*, 832–837.

49. Tan, S. F.; Wu, L.; Yang, J. K. W.; Bai, P.; Bosman, M.; Nijhuis, C. A. Quantum Plasmon Resonances Controlled by Molecular Tunnel Junctions. *Science* **2014**, *343*, 1496–1499.
50. Vogel, N.; Goerres, S.; Landfester, K.; Weiss, C. K. A Convenient Method to Produce Close-and Non-Close-Packed Monolayers Using Direct Assembly at the Air–Water Interface and Subsequent Plasma-Induced Size Reduction. *Macromol. Chem. Phys.* **2011**, *212*, 1719–1734.